MOLECULAR AND CELLULAR BIOLOGY, Aug. 2005, p. 7333–7343 Vol. 25, No. 16
0270-7306/05/$08.00+0 doi:10.1128/MCB.25.16.7333–7343.2005

Defining the Domains of Human Polynucleotide Phosphorylase (hPNPase^{OLD-35}) Mediating Cellular Senescence

Devanand Sarkar,[1] Eun Sook Park,[1] Luni Emdad,[1] Aaron Randolph,[2] Kristoffer Valerie,[2] and Paul B. Fisher[1,3,4]*

Departments of Pathology,[1] Neurosurgery,[3] and Urology,[4] Herbert Irving Comprehensive Cancer Center, Columbia University, College of Physicians and Surgeons, New York, New York 10032, and Department of Radiation Oncology, Medical College of Virginia, Virginia Commonwealth University, Richmond, Virginia 23298[2]

Received 3 December 2004/Returned for modification 24 February 2005/Accepted 24 May 2005

To fully comprehend cellular senescence, identification of relevant genes involved in this process is mandatory. Human polynucleotide phosphorylase (hPNPase^{OLD-35}), an evolutionarily conserved 3′, 5′ exoribonuclease mediating mRNA degradation, was first identified as a predominantly mitochondrial protein overexpressed during terminal differentiation and senescence. Overexpression of hPNPase^{OLD-35} in human melanoma cells and melanocytes induces distinctive changes associated with senescence, potentially mediated by direct degradation of c-*myc* mRNA by this enzyme. hPNPase^{OLD-35} contains two RNase PH (RPH) domains, one PNPase domain, and two RNA binding domains. Using deletion mutation analysis in combination with biochemical and molecular analyses we now demonstrate that the presence of either one of the two RPH domains conferred similar functional activity as the full-length protein, whereas a deletion mutant containing only the RNA binding domains was devoid of activity. Moreover, either one of the two RPH domains induced the morphological, biochemical, and gene expression changes associated with senescence, including degradation of c-*myc* mRNA. Subcellular distribution confirmed hPNPase^{OLD-35} to be localized both in mitochondria and the cytoplasm. The present study elucidates how a predominantly mitochondrial protein, via its localization in both mitochondria and cytoplasm, is able to target a specific cytoplasmic mRNA, c-*myc*, for degradation and through this process induce cellular senescence.

RNases are enzymes that are master regulators of stability and decay of RNA (7–9). Depending upon their degradative characteristics, RNases are divided into two functional classes, endo- and exoribonucleases (8). In *Escherichia coli*, there are eight distinct exoribonucleases, of which two, RNase PH (RPH) and polynucleotide phosphorylase (PNPase), catalyze RNA degradation only in a phosphate-dependent manner (2, 8). In vivo, PNPase catalyzes mRNA decay in the 3′-5′ direction, while RPH is primarily involved in 3′ processing of tRNA precursors (15, 22, 29, 30). RPHs are proteins of ~250 amino acid (aa) residues, whereas PNPase is a large molecule that contains two RPH domains separated by an α-helix (PNPase domain) and two COOH-terminal RNA binding domains, KH and S1 (29, 37, 38, 42).

The structure of PNPase containing the five motifs is conspicuously preserved through evolution extending from prokaryotes and plants to mammals (23). In *E. coli*, PNPase to a small degree functions as a constituent of the degradosome, a multiprotein complex also consisting of RNase E, RNA helicase, enolase, and possibly other molecules (4). However, PNPase in the chloroplast forms a homotrimeric complex (2), and X-ray crystallographic analysis of the PNPase from the bacterium *Streptomyces antibioticus* also reveals a homotrimeric complex forming a "doughnut" shape surrounding a central channel capable of accommodating a single-stranded RNA molecule (37, 38). In addition to the characteristic five motifs, plant PNPase contains an N-terminal target peptide allowing translocation to chloroplasts and the mammalian PNPase contains an N-terminal mitochondrial localization signal facilitating its subcellular localization in mitochondria (28, 31, 40).

Cloning of human polynucleotide phosphorylase was first achieved using an overlapping pathway screening (OPS) strategy designed to identify genes involved in the processes of cellular differentiation and senescence (24). Human melanoma HO-1 cells undergo terminal cell differentiation resembling melanocytes when treated with fibroblast beta interferon (IFN-β) and the protein kinase C activator mezerein (MEZ) (11–13, 16, 21). Senescence is a state of irreversible growth arrest induced spontaneously in primary cells after a finite number of population doublings (replicative senescence) or induced by endogenous and exogenous acute and chronic stress signals (stress- or aberrant-signaling-induced senescence) (17, 34). Although terminal cell differentiation in HO-1 cells by IFN-β plus MEZ and cellular senescence represent two discrete phenomena, there are several overlapping characteristics of these processes. Both are distinguished by irreversible growth arrest associated with marked inhibition of DNA synthesis, inhibition of telomerase activity, and modulation of gene expression, especially up-regulation of cyclin-dependent kinase inhibitors (CDKI) (3, 12, 17, 21, 32). Screening of a temporal cDNA library generated from terminally differentiated HO-1 cells with cDNAs from senescent progeroid fibroblasts identified 75 genes, termed *old*-1 to -75, that were upregulated during terminal differentiation and senescence (24). Sequence analysis of one particular clone, *old*-35, con-

* Corresponding author. Mailing address: Department of Pathology, College of Physicians & Surgeons, Columbia University, 630 W. 168th St., P&S Box 23, BB-1501, New York, NY 10032. Phone: (212) 305-3642. Fax: (212) 305-8177. E-mail: pbf1@columbia.edu.

firmed identity to the PNPase gene, resulting in the gene being renamed *hPNPase$^{old\text{-}35}$* (24).

hPNPase$^{old\text{-}35}$ is an early type I interferon-inducible gene, and its expression is augmented in senescent progeroid fibroblasts in comparison to actively proliferating young counterparts (24, 25). In vitro assays confirmed the phosphate-dependent RNA degradation properties of hPNPase$^{OLD\text{-}35}$, thus confirming the structural and functional conservation of this molecule through evolution (24). Interestingly, overexpression of *hPNPase$^{old\text{-}35}$* via an adenoviral vector in HO-1 cells promotes a senescence-like phenotype characterized by growth arrest in the G_1 phase, inhibition of DNA synthesis and telomerase activity, and modulation of gene expression, most notably downregulation of c-*myc* and upregulation of CDKI p27^{KIP1} (32). In vitro assays documented that c-*myc* mRNA is specifically degraded by hPNPase$^{OLD\text{-}35}$, thus revealing a specific mRNA substrate for hPNPase$^{OLD\text{-}35}$ (32).

The present study examines the different motifs of hPNPase$^{OLD\text{-}35}$ and their roles in mediating its senescence-inducing properties. We observed that either of the RPH domains is capable of inducing the morphological, biochemical, and gene expression changes leading to the senescence phenotype. This is the first demonstration of functional activity and specificity of discrete domains of hPNPase$^{OLD\text{-}35}$ molecule, which will now pave the way for an in-depth understanding of this intriguing molecule as well as permitting a comparative functional analysis of the domains of PNPase molecules in different species.

MATERIALS AND METHODS

Cell lines and culture conditions. The human metastatic melanoma cell line HO-1 and the human embryonic kidney cell line HEK-293 were cultured in Dulbecco's modified Eagle medium supplemented with 10% fetal bovine serum, 50 units/ml penicillin G, and 50 μg/ml streptomycin at 37°C in 5% CO_2 and 100% relative humidity. HO-1 cells were cultured with IFN-β at a dose of 1,000 units/ml for 2 days to detect hPNPase$^{OLD\text{-}35}$.

Plasmid construction. All plasmids were constructed in a backbone of pcDNA3.1+(Hygro) (Invitrogen, Carlsbad, CA) into the NheI and BamHI sites, and all the constructs contained a COOH-terminal hemagglutinin (HA) tag. phPNPase$^{old\text{-}35}$, expressing the full-length hPNPase$^{OLD\text{-}35}$ protein, was amplified by PCR using the cloned *hPNPase$^{old\text{-}35}$* cDNA as a template (24) and primers sense(1), 5′-GCTAGCATGGCGGCCTGCAGGTAC-3′, and antisense(1), 5′-GGATCCTCAAGCGTAATCTGGAACATCGTATGGGTACTGAGAATTAGATGATGA-3′. pΔRPH1 was created by PCR using primers sense(2), 5′-GCTAGCATGCCTTGGAATGGACCTGTTGGG-3′, and antisense(1). pΔRPH2 was cloned in two steps. First, a 3′ PCR fragment was amplified by PCR using primers sense(3), 5′-GTTAACATGGATTCAGGGGTTCCAATT-3′, and antisense(1) and ligated to pGEMT-easy vector (Promega, Madison, WI) by TA cloning. This fragment was digested with HpaI and BamHI and ligated into HpaI- and BamHI-digested phPNPase$^{old\text{-}35}$. pΔRPH1+2 was generated by PCR using primer sense(4), 5′-GCTAGCATGGATTCAGGGGTTCCAATT-3′, and antisense(1). pΔC-term was generated by PCR using primers sense(1) and antisense(2), 5′-GGATCCTCAAGCGTAATCTGGAACATCGTATGGGTACTGCAACAGCAGATGAAATTGG-3′. The authenticity of all the constructs was confirmed by sequencing. The PCR fragments were first cloned into the vector pGEMT-easy by TA cloning and then transferred to pcDNA3.1+(Hygro). The c-*myc* expression plasmid [p290-myc(2,3)] was provided by Riccardo Dalla-Favera (Columbia University Medical Center, New York, NY).

Virus construction and infection protocol. The construction of *hPNPase$^{old\text{-}35}$* expressing replication-defective Ad.*hPNPase$^{old\text{-}35}$* was performed by cloning the transgene into a shuttle vector (p0TgCMV) and then performing homologous recombination of the shuttle vector with a parental adenoviral vector having the E1 and E3 regions deleted in *E. coli* as described previously (18, 24). A similar method was employed to generate Ad.Δ*RPH1*, Ad.Δ*RPH2*, Ad.Δ*RPH1+2*, and Ad.Δ*C-term*. The transgene was digested from the pGEMT-easy vector with NotI and ligated into the NotI site of p0TgCMV. The direction of the cloning was confirmed by restriction enzyme digestion and sequencing. The empty adenoviral vector (Ad.*vec*) was used as a control. The adenovirus (Ad) was propagated in HEK293 cells (18) and purified by BD AdenoX virus purification kit (BD Biosciences, Palo Alto, CA), and viral titer was determined by measuring optical density at 260 nm and using BD AdenoX rapid titer kit (BD Biosciences). Ad infection was performed 24 h after cell plating in one-fifth the volume of the original culture medium in a serum-free condition for 2 h with rocking the plates several times (18).

Colony formation assays. HO-1 cells were plated at a density of 3×10^5 cells per 6-cm dish and 24 h later were infected with different Ads at multiplicities of infection (MOI) of 10, 20, and 50 PFU/cell. For colony formation assays with c-*myc* overexpression, HO-1 cells were plated at a density of 3×10^5 cells per 6-cm dish and 24 h later were transfected with 5 μg of either empty vector or p290-myc (2, 3) using Superfect (QIAGEN, Hilden, Germany) transfection reagent according to the manufacturer's protocol. After 36 h, the cells were infected with different Ads at an MOI of 50 PFU/cell. Six hours after infection, the cells were trypsinized and counted, and 10^3 cells were plated in 6-cm dishes. Colonies of >50 cells were counted after 2 weeks.

Western blot analysis. Western blotting was performed as previously described (33). Briefly, cells were harvested in radioimmunoprecipitation assay (RIPA) buffer (1× phosphate-buffered saline [PBS], 1% NP-40, 0.5% sodium deoxycholate, 0.1% sodium dodecyl sulfate [SDS]) containing a protease inhibitor cocktail (Roche, Mannheim, Germany), 1 mM Na_3VO_4, and 50 mM NaF and centrifuged at 12,000 rpm for 10 min at 4°C. The supernatant was used as total cell lysate. Thirty micrograms of total cell lysate was used for SDS-polyacrylamide gel electrophoresis and transferred to a nitrocellulose membrane. The primary antibodies included Myc (1:200; mouse monoclonal), Max (1:200; rabbit polyclonal), Mad1 (1:200; rabbit polyclonal), p21 (1:200; rabbit polyclonal), p27 (1:200; rabbit polyclonal), and CDK2 (1:250; rabbit polyclonal) (Santa Cruz Biotechnology, Santa Cruz, CA); p16 (1:500; mouse monoclonal), Rb (1:500; mouse monoclonal), actin (1:1,000; mouse monoclonal), cytochrome *c* (1:1,000; mouse monoclonal), and cyclin B1 (1:5,000; mouse monoclonal) (BD Biosciences); anti-hPNPase$^{OLD\text{-}35}$ (1:10,000; chicken polyclonal) (31); anti-HA (1:1,000; mouse monoclonal; Covance Research Products, Inc., Berkeley, CA); and EF1α (1:1,000; mouse monoclonal; Upstate Biotechnology, Waltham, MA).

Immunofluorescence analysis. HO-1 cells were plated on chamber slides (Falcon 4102; Becton Dickinson, Franklin Lakes, NJ) and infected with different Ads. After 36 h, the cells were loaded with 250 nM MitoTracker (Molecular Probes, Eugene, OR) for 30 min at 37°C, fixed with 3.7% formaldehyde for 15 min at 37°C, and permeabilized with 0.1% Triton X-100 in PBS for 5 min at room temperature (RT). The cells were blocked with PBS containing 10% normal rabbit serum for 2 h at RT and incubated in the blocking solution containing anti-HA antibody (1:200) overnight at 4°C. After washing in PBS, the cells were incubated in the blocking solution containing anti-mouse-fluorescein isothiocyanate (FITC; 1:200) for 2 h at RT, washed again in PBS, mounted, and visualized using a Zeiss confocal laser scanning microscope (LSM510) and a 40× objective. In case of double-immunofluorescence studies for hPNPase$^{OLD\text{-}35}$ and p27$^{KIP\text{-}1}$, HO-1 cells were plated on chamber slides and infected with Ad.*hPNPase$^{old\text{-}35}$* and 48 h later they were fixed, permeabilized, and blocked with PBS containing 5% normal goat serum. The cells were incubated first with anti-p27 antibody and Alexa Fluor 594 (red) goat anti-rabbit immunoglobulin G (IgG; Molecular Probes), followed by anti-hPNPase$^{OLD\text{-}35}$ antibody and rabbit anti-chicken-FITC (Genetel Laboratories, Madison, WI). Image analysis was performed using a Zeiss confocal laser scanning microscope (LSM510) and a 40× objective.

Cell fractionation. Cells (2×10^7) were harvested by trypsinization, and mitochondrial and cytoplasmic fractions were separated using a mitochondrion isolation kit (Pierce, Rockford, IL) according to the manufacturer's protocol.

Assay for SA-β-Gal activity. Senescence-associated β-galactosidase (SA-β-Gal) activity was assayed 4 days after infection with different Ads at an MOI of 50 PFU/cell (10). The cells were fixed with 2% formaldehyde plus 0.2% glutaraldehyde and then stained with X-Gal (5-bromo-4-chloro-3-indolyl-β-D-galactopyranoside; 1 mg/ml) in 40 mM citric acid/Na phosphate buffer (pH 6.0) containing 5 mM potassium ferrocyanide, 5 mM potassium ferricyanide, 150 mM NaCl, and 2 mM $MgCl_2$. After the development of color, the cells were washed with PBS and methanol, air dried, and microphotographed. Quantification of SA-β-Gal-positive cells was determined by counting at least 1,000 cells for each group.

Cell cycle analysis. The cell cycle was analyzed at 1, 2, and 3 days postinfection. Cells were harvested, washed in PBS, and fixed overnight at −20°C in 70% ethanol. Cells were treated with RNase A (1 mg/ml) at 37°C for 30 min and then with propidium iodide (50 μg/ml). The cell cycle was analyzed using a FACSCalibur flow cytometer, and data were analyzed using CellQuest software (Becton Dickinson, San Jose, CA).

Cell sorting analysis. HO-1 cells were transfected with either empty vector or c-*myc* expression plasmid and infected the next day with either Ad.*vec* or Ad.*hPNPase^{old-35}* at an MOI of 50 PFU/cell. Two days after infection, live cells were incubated with 5 μg/ml of Hoechst 33342 (Molecular Probes) for 1 h in the dark. After trypsinization, cells were resuspended at a concentration of 10^7 cells/ml for sorting. Cells were sorted based on the amount of DNA by defining three regions for sorting: one for G_1, one for S, and one for G_2+M using BDFACSAria (BD Biosciences) equipped with a UV laser required for Hoechst 33342 excitation. The separated cells (at least 10^6 cells from each sorted population) were collected, protein was extracted, and Western blot analysis was performed.

RNA isolation and Northern blot analysis. Total RNA was extracted from the cells using the QIAGEN RNeasy minikit according to the manufacturer's protocol, and Northern blotting was performed as described previously (33). The cDNA probes used were a 500-bp fragment from human c-*myc*, full-length human GADD34, and full-length human GAPDH (glyceraldehyde-3-phosphate dehydrogenase).

In vitro translation and in vitro mRNA degradation assays. In vitro translation was performed using the TNT coupled reticulocyte lysate systems (Promega) using the plasmids pcDNA3.1+(Hygro) (as a control), GADD153 expression plasmid, phPNPase^{old-35}, pΔRPH1, pΔRPH2, pΔRPH1+2, and pΔC-term according to the manufacturer's protocol. Five micrograms of total RNA from HO-1 cells was incubated with 5 μl of each in vitro-translated protein at 37°C from 0.5 to 2 h. The RNA was repurified using the QIAGEN RNeasy minikit, and Northern blotting was performed.

CDK activity assay. Cells were harvested in RIPA buffer, and 500 μg of protein was incubated overnight at 4°C with anti-CDK2 antibody and then with protein A agarose for 1 h at 4°C. The agarose beads were spun down at 10,000 × *g* for 5 min and washed three times in RIPA buffer and once in kinase buffer. The immunoprecipitated material was employed for kinase assays using histone H1 (Upstate Biotechnology) as the substrate and [γ-^{32}P]ATP (Amersham, Piscataway, NJ) in a kinase buffer containing 25 mM Tris-HCl, pH 7.5, 150 mM NaCl, 18 mM $MgCl_2$, and 1 mM dithiothreitol for 30 min at 30°C. Following the reaction the samples were subjected to 15% SDS-polyacrylamide gel electrophoresis, the gel was dried and exposed to X-ray film, and densitometric analysis was performed.

Statistical analysis. Statistical analysis was performed using one-way analysis of variance, followed by Fisher's protected least significant difference analysis.

RESULTS

Polynucleotide phosphorylases are highly conserved across species ranging from bacteria and plants to mammals (23). They have a conventional structure containing RNase PH domains and RNA binding domains (37, 38). Figure 1A (top panel) shows the different domains of hPNPase^{OLD-35}. hPNPase^{OLD-35} contains 783 amino acid residues. The first 45 aa contain a mitochondrial localization signal. Interestingly, the bacterial PNPase does not contain such a signal, whereas the plant PNPase contains a chloroplast localization signal, suggesting possible evolutionary divergence of this gene in eukaryotes. hPNPase^{OLD-35} contains two RNase PH (RPH) domains, involved in RNA degradation, one at aa 52 to 183, the other at aa 366 to 501. Between the two RPH domains there is an α-helix at aa 289 to 363 that is unique for PNPase and is involved in RNA binding. There are two RNA binding domains at the COOH terminal of the molecule: the KH domain is at aa 605 to 667, and the S1 domain is at aa 676 to 750.

In order to comprehend the involvement of these domains in mediating the hPNPase^{OLD-35}-induced senescence phenotype, a number of deletion mutants were created and replication-incompetent Ads expressing these deletion mutants were generated (Fig. 1A). All the constructs were tagged with a C-terminal HA epitope (YPYDVPDYA) for monitoring the site and level of expression of the proteins. Ad.*hPNPase^{old-35}* contains the product of the complete open reading frame of *hPNPase^{old-35}*; Ad.Δ*RPH1* contains aa 183 to 783 lacking the mitochondrial localization signal and RPH1 domain; Ad.Δ*RPH2* contains aa 1 to 202 and 496 to 783 lacking the PNPase and RPH2 domains; Ad.Δ*RPH1+2* contains aa 496 to 783 lacking the mitochondrial localization signal, both RPH domains, and PNPase domain; and Ad.Δ*C-term* contains aa 1 to 507 lacking the KH and S1 RNA binding domains. The predicted molecular masses of the proteins generated from these constructs are 86, 67, 54, 31, and 55 kDa for the *hPNPase^{OLD-35}* protein, ΔRPH1, ΔRPH2, ΔRPH1+2, and ΔC-term, respectively, which was confirmed by Western blotting (data not shown).

It was considered important to initially determine if the level of expression of *hPNPase^{old-35}* resulting from adenoviral delivery of this gene was comparable to the level of endogenous protein induced following IFN-β treatment. To address this issue, HO-1 cells were infected with either Ad.*vec* (control empty Ad) or with Ad.*hPNPase^{old-35}* at an MOI of 50 PFU/cell or treated with 1,000 units/ml of IFN-β and the expression of *hPNPase^{OLD-35}* was analyzed 2 days later by Western blot analysis using anti-hPNPase^{OLD-35} antibody (31). Treatment with IFN-β resulted in marked induction of hPNPase^{OLD-35}, and the level of the protein generated upon Ad.*hPNPase^{old-35}* infection was approximately twofold more than that with IFN-β treatment (Fig. 1B). These findings indicate that Ad.*hPNPase^{old-35}* generates hPNPase^{OLD-35} that is within a physiological range, and the effects observed with Ad.*hPNPase^{old-35}* infection represent potentially physiologically relevant events.

To analyze the involvement of the different domains in hPNPase^{OLD-35}-induced growth inhibition and senescence, HO-1 human melanoma cells were infected with the different Ads at MOIs of 10, 20, and 50 PFU/cell and colony formation assays were performed. As a control, cells were either uninfected or infected with Ad.*vec* at an MOI of 50 PFU/cell. As shown in Fig. 1C, infection with Ad.*hPNPase^{old-35}*, Ad.Δ*RPH1*, Ad.Δ*RPH2*, and Ad.Δ*C-term* resulted in a dose-dependent inhibition in growth. At an MOI of 50 PFU/cell colony formation was reduced by 60%, 54%, 51%, and 51% upon infection with Ad.*hPNPase^{old-35}*, Ad.Δ*RPH1*, Ad.Δ*RPH2*, and Ad.Δ*C-term*, respectively. On the other hand, infection with Ad.*vec* or Ad.Δ*RPH1+2* did not result in any significant growth inhibition. These findings confirm that retention of only the C-terminal RNA binding domains is not adequate, whereas either of the RPH domains is sufficient for mediating growth inhibition. The observation that Ad.Δ*C-term* also has potent growth-inhibiting properties indicates that the PNPase RNA binding domain might be sufficient for RNA binding and subsequent RPH activation.

To determine the senescence-inducing properties of these deletion mutants, HO-1 cells were infected with the different Ads and monitored for changes in cell morphology and SA-β-Gal activity, a characteristic marker of senescence (10). Infection with Ad.*hPNPase^{old-35}*, Ad.Δ*RPH1*, Ad.Δ*RPH2*, and Ad.Δ*C-term*, but not Ad.*vec* and Ad.Δ*RPH1+2*, resulted in typical morphological changes in HO-1 cells (Fig. 1D). Large, flattened cells that stained for SA-β-Gal were observed (white arrows). In Ad.*vec*- and Ad.Δ*RPH1+2*-infected cells 7 and 6% of the cells, respectively, stained positive for SA-β-Gal while in Ad.*hPNPase^{old-35}*, Ad.Δ*RPH1*, Ad.Δ*RPH2*, and Ad.Δ*C-term*-infected cells 35, 28, 45, and 29% of the cells, respectively,

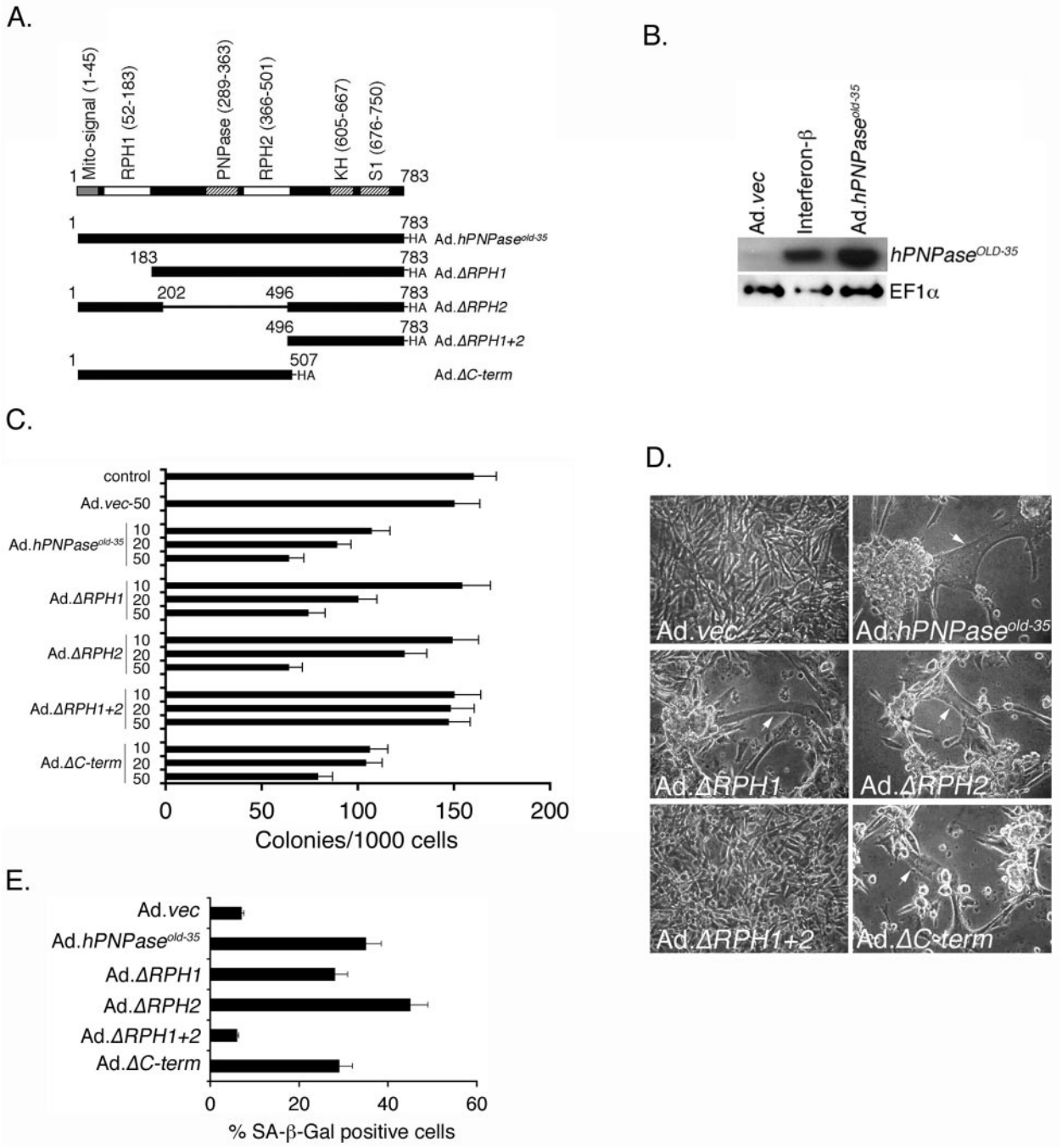

FIG. 1. The RPH domain of hPNPase^{OLD-35} is required for induction of senescence in HO-1 cells. A. Schematic representation of the domain structure of hPNPase^{OLD-35} and the different deletion mutants. The numbers represent the amino acid numbers. The gray box is the mitochondrial localization signal, white boxes are the RPH domains, and the hatched boxes are the RNA binding domains. B. HO-1 cells were either infected with the indicated Ad at an MOI of 50 PFU/cell or treated with beta interferon at a dose of 1,000 units/ml, and the levels of the indicated proteins were analyzed by Western blot analysis 48 h later. C. HO-1 cells were either uninfected or infected with Ad.*vec* at an MOI of 50 PFU/cell or with the indicated Ad at an MOI of 10, 20, or 50 PFU/cell, and colony formation assays were determined as described in Materials and Methods. The data represent means ± standard deviations (SD) and are a representation of three independent experiments, each performed in triplicate. D. Microphotograph of HO-1 cells infected with the indicated Ad at an MOI of 50 PFU/cell 4 days postinfection. The white arrows indicate the large, flattened cells that stain for SA-β-Gal. E. Quantification of SA-β-Gal-positive cells. At least 1,000 cells were counted for each group. The data represent means ± SD of three independent experiments.

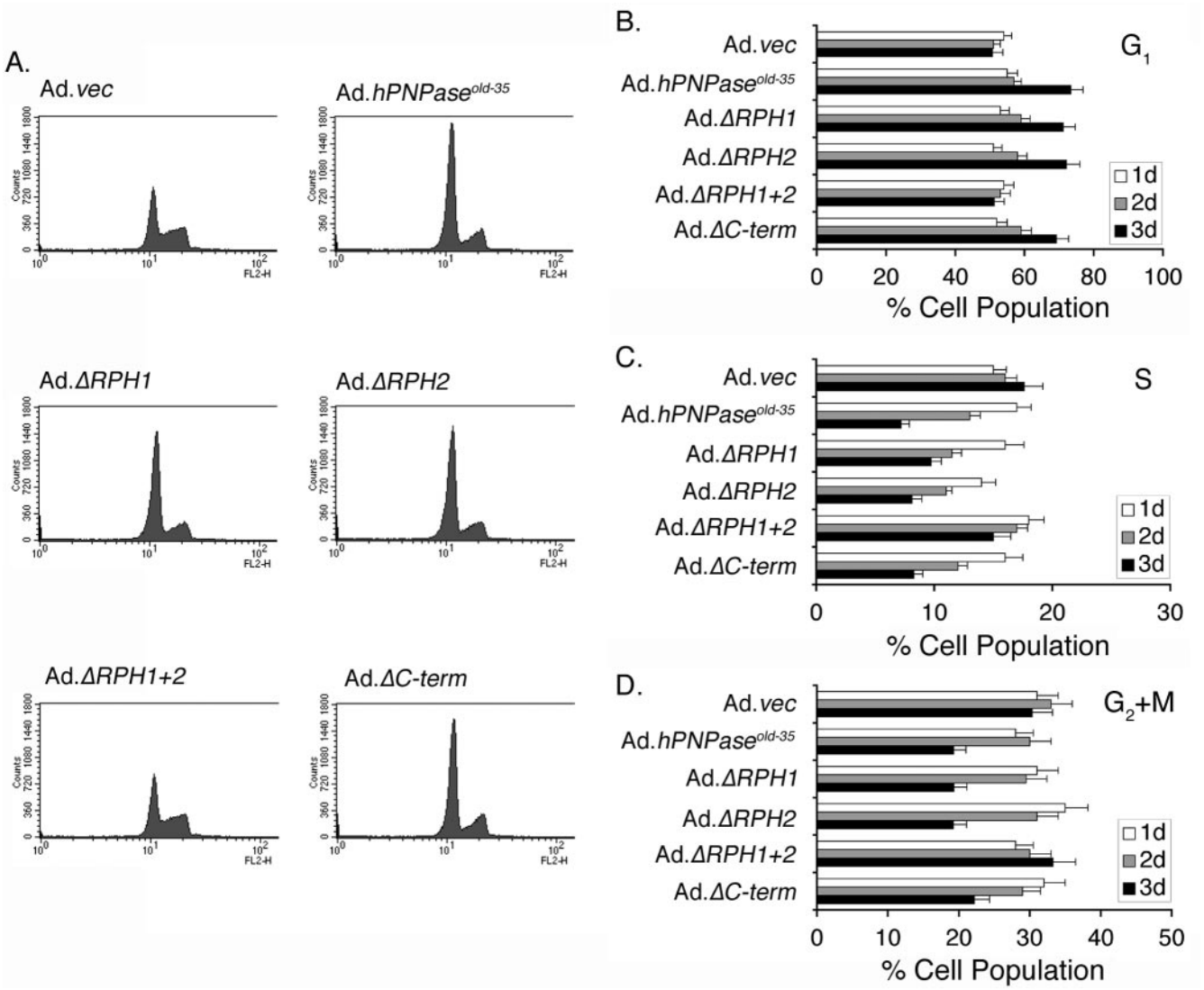

FIG. 2. hPNPase^{OLD-35} and its RPH-containing deletion mutants inhibit the cell cycle at the G_1 phase. HO-1 cells were infected with the indicated Ad at an MOI of 50 PFU/cell, and the cell cycle was analyzed on days 1, 2, and 3 postinfection. A. Flow cytometry histogram of cells infected with the indicated Ad 3 days postinfection. B to D. Graphical representation of the percentage of cells in the G_1 (B), S (C), and G_2+M (D) phases of the cell cycle. The data represent means ± standard deviations of three independent experiments.

displayed SA-β-Gal positivity (Fig. 1E). These findings indicate that similar to growth inhibition the morphological and biochemical changes, characteristic of senescence and induced by *hPNPase^{old-35}*, also require at least one of the two RPH domains.

Senescence is associated with arrest of the cell cycle especially at the G_1 phase, with a decrease in the S phase indicative of inhibition of DNA synthesis (35). Cell cycle analysis was performed in HO-1 cells infected with the different Ads. A time-dependent change in the cell cycle pattern was observed (Fig. 2A to D). Three days after infection, 51% of the cells were in the G_1 phase following Ad.*vec* and Ad.Δ*RPH1+2* infection. At the same time point, 73%, 71%, 72%, and 69% of the cells were in the G_1 phase following Ad.*hPNPase^{old-35}*, Ad.Δ*RPH1*, Ad.Δ*RPH2*, and Ad.Δ*C-term* infection, respectively. Similarly, while 17% and 15% of the cells were in the S phase following Ad.*vec* and Ad.Δ*RPH1+2* infection, respectively, 7%, 9%, 8%, and 8% of the cells were in the S phase following Ad.*hPNPase^{old-35}*, Ad.Δ*RPH1*, Ad.Δ*RPH2*, and Ad.Δ*C-term* infection, respectively. These findings corroborate the findings of SA-β-Gal staining that growth arrest in the G_1 phase and inhibition of DNA synthesis induced by hPNPase^{OLD-35} also require the RPH domain.

We next investigated the expressions of proteins that regulate the progression of the cell cycle beyond the G_1 phase by Western blot analysis. There was a significant increase in p27^{KIP1} and a decrease in p21$^{CIP1/WAF-1/MDA-6}$ upon infection with Ad.*hPNPase^{old-35}*, Ad.Δ*RPH1*, Ad.Δ*RPH2*, and Ad.Δ*C-term*, but not with Ad.*vec* and Ad.Δ*RPH1+2* (Fig. 3A). No p16^{INK4A} protein was detected in HO-1 cells, which is due to the fact that a majority of melanomas have genomic abnormalities in the p16^{INK4A} gene (5). The level of phosphorylated Rb

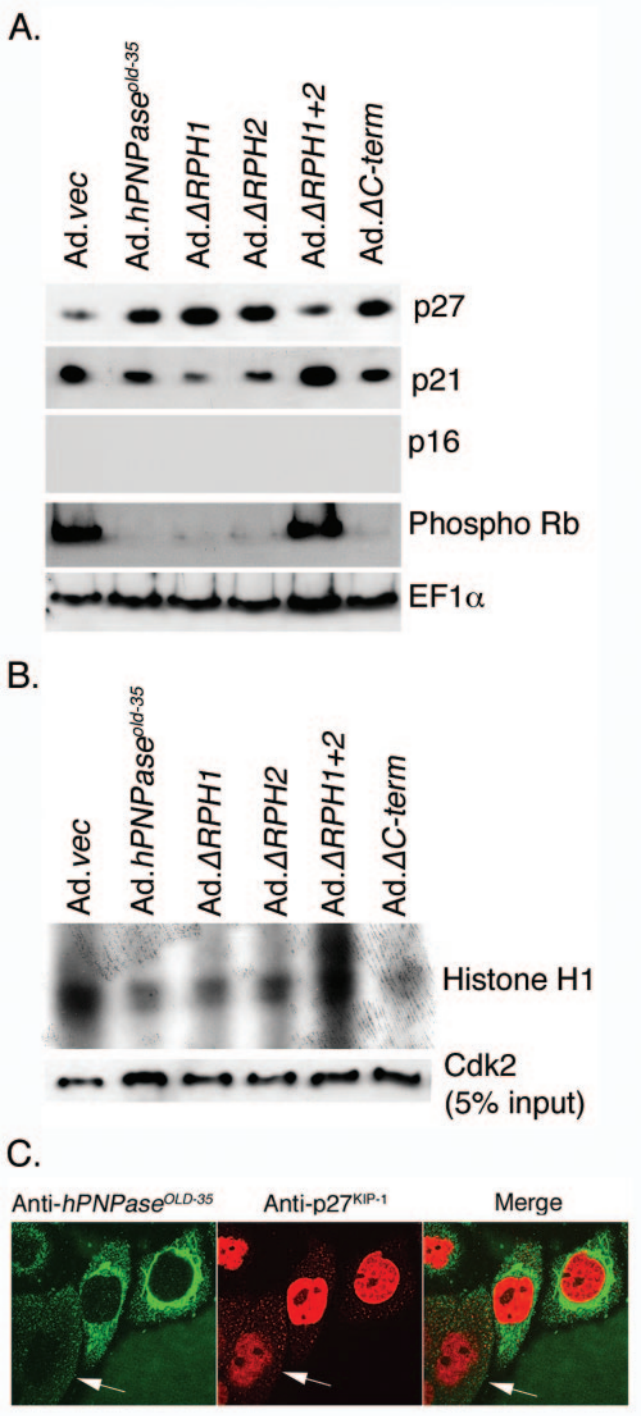

FIG. 3. Regulation of expression of cell cycle regulatory proteins by hPNPase^{OLD-35} and its deletion mutants. A. HO-1 cells were infected with the indicated Ad at an MOI of 50 PFU/cell for 3 days, and the expression of the indicated proteins in the cell lysates was analyzed by Western blot analysis. B. HO-1 cells were treated as in panel A, and CDK2 activity was assayed using histone H1 as substrate as described in Materials and Methods. The expression level of CDK2 in 5% of the input used for the CDK2 activity assay was determined by Western blot analysis. C. HO-1 cells were infected with Ad.*hPNPase*$^{old-35}$ at an MOI of 50 PFU/cell for 2 days, and immunofluorescence studies were performed to analyze the expression of hPNPase^{OLD-35} and p27^{KIP-1} as described in Materials and Methods.

decreased significantly upon infection with Ad.*hPNPase*$^{old-35}$, Ad.Δ*RPH1*, Ad.Δ*RPH2*, and Ad.Δ*C-term*. These findings show that the increase in the level of p27^{KIP1} inhibits cyclin-dependent kinase activity resulting in hypophosphorylation of Rb and arrest of cell cycle in the G_1 phase. This possibility was confirmed by assaying for CDK2 activity by in vitro kinase assays using histone H1 as a substrate. Cell lysates obtained from Ad.*vec* and Ad.Δ*RPH1+2* had high CDK2 kinase activity that was markedly reduced in cell lysates obtained from Ad.*hPNPase*$^{old-35}$-, Ad.Δ*RPH1*-, Ad.Δ*RPH2*-, and Ad.Δ*C-term*-infected cells (Fig. 3B). The levels of CDK2 itself were similar in all the samples indicating that the decrease in the CDK2 activity is not because of a decrease in CDK2 itself, but a consequence of upregulation of the CDKI p27^{KIP1} (Fig. 3B). The relationship between Ad.*hPNPase*$^{old-35}$ infection and p27^{KIP1} upregulation was further documented by double-immunofluorescence analysis. The cells expressing no *hPNPase*$^{OLD-35}$ showed a basal level of p27^{KIP1} expression (Fig. 3C, arrows), while *hPNPase*$^{OLD-35}$-expressing cells displayed higher levels of p27^{KIP1} (Fig. 3C).

It was documented previously that downregulation of c-*myc* plays a significant role in mediating *hPNPase*$^{old-35}$-induced growth inhibition (32). Considering this possibility, the involvement of the domains of hPNPase^{OLD-35} in regulating c-*myc* expression was analyzed. Infection with Ad.*hPNPase*$^{old-35}$, Ad.Δ*RPH1*, Ad.Δ*RPH2*, and Ad.Δ*C-term*, but not with Ad.*vec* and Ad.Δ*RPH1+2*, resulted in ~50% reduction in c-*myc* mRNA level 3 days postinfection (Fig. 4A and B). This reduction was also reflected at the level of the MYC protein (Fig. 4C). The expression of MYC protein decreased, while that of MAD-1 protein increased significantly, following Ad.*hPNPase*$^{old-35}$, Ad.Δ*RPH1*, Ad.Δ*RPH2*, and Ad.Δ*C-term* infection, but not with Ad.*vec* and Ad.Δ*RPH1+2* infection. The level of MAX and EF1α remained unchanged under all treatment protocols. These findings indicate that the RPH domains of hPNPase^{OLD-35} are required to downregulate c-*myc* expression, which results in a switch from a MYC-MAX transcriptional activator to MAD-1-MAX transcriptional repressor.

To support the observations of these expression studies, c-*myc* was overexpressed in HO-1 cells and these cells were infected with the different Ads and colony-forming ability was determined. Infection with Ad.*hPNPase*$^{old-35}$, Ad.Δ*RPH1*, Ad.Δ*RPH2*, and Ad.Δ*C-term* decreased colony formation by 75%, 73%, 79%, and 74%, respectively, in comparison to infection with Ad.*vec* and Ad.Δ*RPH1+2* (Fig. 4D). Overexpersion of c-*myc* provided partial but significant protection so that colony formation was decreased by 46%, 44%, 53%, and 46% upon infection with Ad.*hPNPase*$^{old-35}$, Ad.Δ*RPH1*, Ad.Δ*RPH2*, and Ad.Δ*C-term*, respectively. These findings suggest that downregulation of c-*myc* plays a prominent role in *hPNPase*$^{old-35}$-mediated growth inhibition.

hPNPase^{OLD-35} is a 3′,5′ exoribonuclease (24), so we investigated whether the downregulation of c-*myc* is a consequence of direct degradation of c-*myc* mRNA by hPNPase^{OLD-35}. hPNPase^{OLD-35} and its different deletion mutants were in vitro translated, and the proteins were used for RNA degradation assays. As shown in Fig. 5A, the plasmid constructs phPNPase^{old-35}, pΔRPH1, pΔRPH2, pΔRPH1+2, and pΔC-term give rise to proteins of the expected molecular masses of 86, 67, 54, 31, and

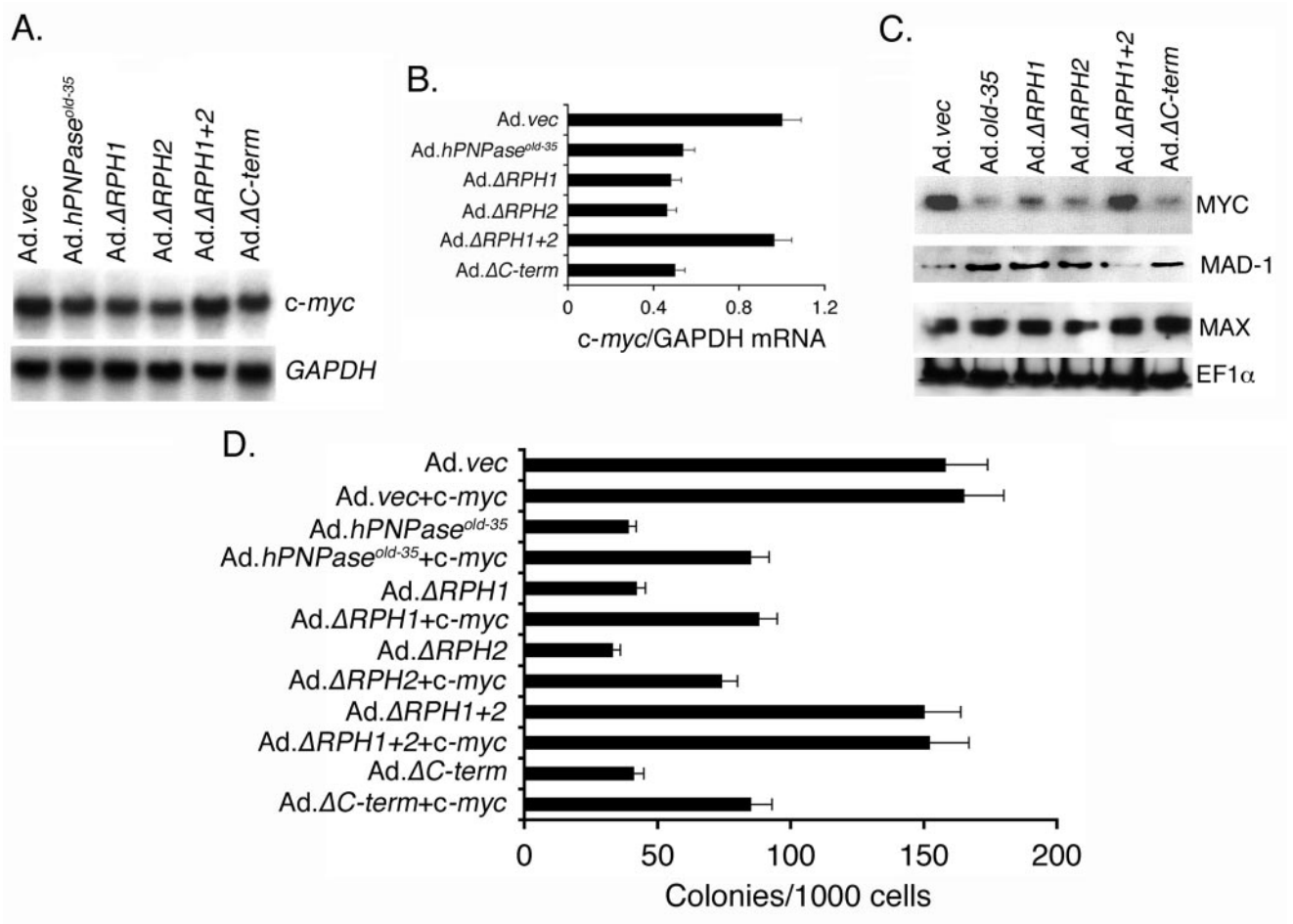

FIG. 4. The RPH domain of hPNPase^{OLD-35} is required for c-*myc* downregulation. A. HO-1 cells were treated as for Fig. 3A, and the expression of the indicated mRNAs was analyzed by Northern blot analysis. B. Graphical representation of the c-*myc*/GAPDH mRNA levels in the indicated treatment groups. The data represent means ± standard deviations (SD) of three independent experiments. C. HO-1 cells were treated as for Fig. 3A, and the expression of the indicated proteins was analyzed by Western blot analysis. D. HO-1 cells were transfected either with an empty vector or with a c-*myc* expression vector and, 36 h later, infected with the indicated Ad at an MOI of 50 PFU/cell, and colony formation assays were performed. The data represent the means ± SD and are a representation of three independent experiments, each performed in triplicate.

55 kDa, respectively, indicating the authenticity of the constructs. The in vitro-translated proteins were incubated with total RNA for 0.5 and 2 h. The RNA was purified, and the expression of c-*myc*, GADD34, and GAPDH mRNAs was analyzed by Northern blot analyses. Incubation with phPNPase^{old-35}, pΔRPH1, pΔRPH2, and pΔC-term resulted in significant degradation of c-*myc* mRNA (Fig. 5B and C). No degradation was observed upon incubation with the control plasmid pcDNA3.1, pΔRPH1+2, and unrelated plasmid pGADD153, which expresses a transcription factor. The expressions of GADD34 and GAPDH mRNAs remained unchanged under all experimental conditions. These findings indicate that the presence of either RPH domain is necessary and sufficient to degrade c-*myc* mRNA, and degradation is specific for c-*myc* mRNA.

To establish a direct correlation between cell cycle arrest in the G_1 phase and c-*myc* downregulation by hPNPase^{OLD-35}, HO-1 cells were sorted following Ad.*hPNPase^{old-35}* infection and the expressions of hPNPase^{OLD-35} and Myc were analyzed in the different phases of the cell cycle (Fig. 6). As a control for authenticity of the sorting procedure the expression of cyclin B1 was analyzed. Cyclin B1 starts being synthesized in late G_1, and its expression is maximum in G_2+M phase, which was confirmed by our cyclin B1 expression analysis in different phases of the cell cycle, indicating the effectiveness of the sorting procedure (Fig. 6, fourth panel from the top). The equal expression of EF1-α in all the samples served as a loading control (Fig. 6, third panel). Although hPNPase^{OLD-35} could be detected in the cells in S and G_2+M phases, significantly higher levels of hPNPase^{OLD-35} were detected in cells in the G_1 phase of the cell cycle following Ad.*hPNPase^{old-35}* infection (Fig. 6, first panel, lanes 4 and 10 versus 5, 6, 11, and 12). The level of hPNPase^{OLD-35} in different phases of the cell cycle inversely correlated with the level of Myc, which was markedly downregulated in cells in the G_1 phase (Fig. 6, second panel, lane 1 versus 4) and moderately downregulated in the cells in S and G_2+M phases (Fig. 6, second panel, lanes 2 and 3 versus 5 and 6) following Ad.*hPNPase^{old-35}* infection. When Myc was overexpressed in cells, there was a slight reduction of Myc in cells in the G_1 phase upon Ad.*hPNPase^{old-35}*

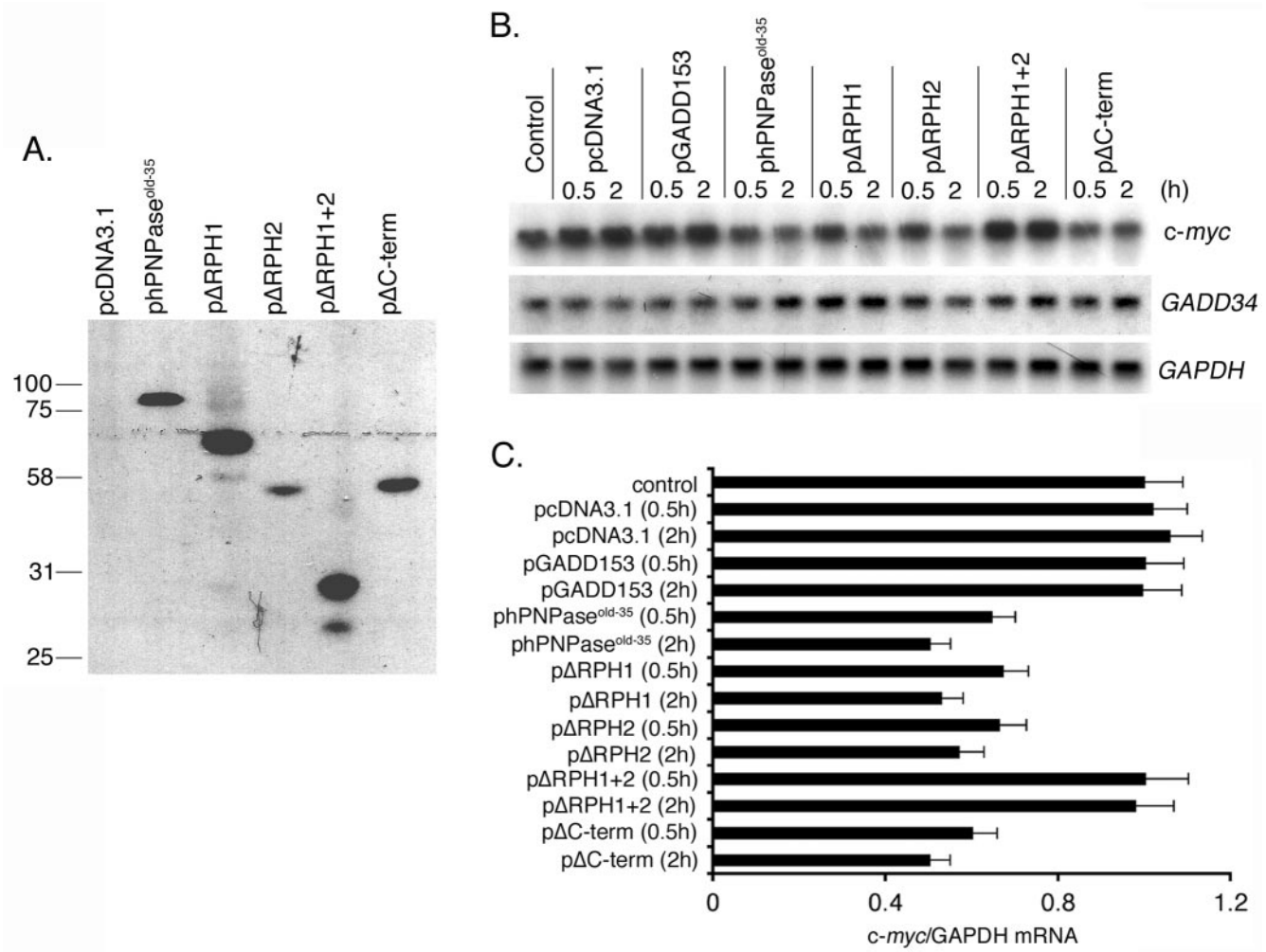

FIG. 5. The RPH domain of hPNPase^{OLD-35} is required for in vitro degradation of c-*myc* mRNA. A. Representation of the in vitro-translated products from the indicated plasmids documenting their authenticity. B. In vitro degradation assays were performed as described in Materials and Methods. The expression of c-*myc*, GADD34, and GAPDH mRNAs was detected by Northern blot analysis. C. Quantification of c-*myc*/GAPDH mRNA levels in the different groups analyzed in panel B. The data represent the means ± standard deviations of three independent experiments.

infection (Fig. 6, second panel, lane 7 versus 10), but this level of Myc was still markedly higher than that in Ad.*hPNPase^{old-35}*-infected G_1 phase cells without Myc overexpression (Fig. 6, second panel, lane 4 versus 10). The decrease of Myc in the Myc-overexpressed G_1 phase cells is probably because of downregulation of endogenous Myc. These findings indicate that hPNPase^{OLD-35} decreases endogenous but not exogenous Myc, thereby explaining the potential protection against hPNPase^{OLD-35} induced growth inhibition by overexpressing Myc. The c-*myc* expression plasmid does not contain the 3′ untranslated region (UTR) of the endogenous mRNA, indicating that the sequence in the 3′ UTR of c-*myc* mRNA might contain a potential binding site for hPNPase^{OLD-35}.

The presence of the mitochondrial localization signal indicates that hPNPase^{OLD-35} is a predominantly mitochondrial protein (28, 31). The question naturally arises as to how a mitochondrial protein might degrade a cytoplasmic mRNA, like c-*myc*. To address this question, cells infected with different Ads were fractionated into mitochondrial and cytoplasmic fractions and the expressions of the proteins were analyzed by Western blotting using anti-HA antibody. As a control for the quality of the purification, membranes were reprobed with anti-actin antibody (for cytoplasmic fraction) and anti-cytochrome *c* antibody (for mitochondria). hPNPase^{OLD-35}, ΔRPH2, and ΔC-term showed predominantly mitochondrial expression resulting from the presence of the mitochondrial localization signal in these constructs (Fig. 7A) while ΔRPH1 and ΔRPH1+2 was located predominantly in the cytoplasmic fraction (Fig. 7A) because of lack of the mitochondrial localization signal. However, high-level expression of hPNPase^{OLD-35} and low-level expression of ΔRPH2 and ΔC-term were also detected in the cytoplasmic fraction and very-low-level expression of ΔRPH1 was detected in the mitochondrial fraction. In the case of hPNPase^{OLD-35}, a smear was detected above the major band, which might result from incomplete denaturation of the homotrimer formed by hPNPase^{OLD-35}. These findings indicate that the proteins are localized both in cytoplasm and mitochondrial compartments and the bands that are detected are

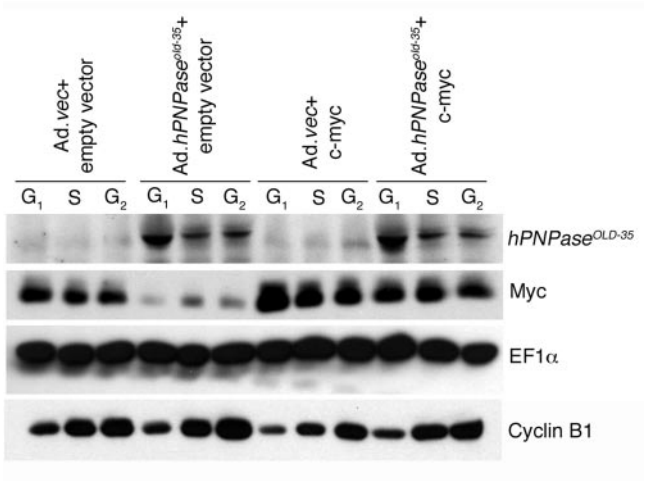

FIG. 6. hPNPase^{OLD-35} downregulates Myc in cells in the G_1 phase of the cell cycle. HO-1 cells were transfected with either empty vector or a c-*myc* expression plasmid and then infected with either Ad.*vec* or Ad.*hPNPase^{old-35}* at an MOI of 50 PFU/cell for 2 days. The cells were sorted as described in Materials and Methods, and the expression levels of the indicated proteins in cells of different phases of cell cycle were analyzed by Western blot analysis. G_2 represents cells in G_2+M phase.

not a consequence of cross-contamination during purification, which is strongly supported by the observation that no cross staining for actin in mitochondria or for cytochrome *c* in cytoplasm was detected.

The fractionation results were confirmed by immunofluorescence studies using anti-HA antibody (green) and MitoTracker (red) to determine the localization of hPNPase^{OLD-35} and its deletion mutants (Fig. 7B). hPNPase^{OLD-35}, ΔRPH2, and ΔC-term showed a speckled expression pattern that colocalized with mitochondrial staining, as evidenced by the presence of yellow in the merged image. However, in addition to the yellow staining, there were also isolated green stainings observed in the merged images, indicating the presence of hPNPase^{OLD-35}, ΔRPH2, and ΔC-term in cytoplasmic compartments. ΔRPH1 and ΔRPH1+2 showed a diffuse expression pattern throughout the cytoplasm that did not colocalize with the mitochondrial staining, indicating the presence of ΔRPH1 and ΔRPH1+2 in the cytoplasm.

DISCUSSION

In this study, the importance of the RPH domains in mediating the characteristic phenotypic changes induced by *hPNPase^{old-35}* is firmly established. We observed that the presence of at least one RPH domain is required for the functional activity of the protein and either of the domains is as potent as the full-length molecule. This contrasts with bacterial PNPase in which mutation in the key residues in either of the RPH domains inhibits catalytic activity (19). However, our result is comparable to chloroplast PNPase in which the first RPH domain alone (comparable to our ΔRPH2 construct) is highly active enzymatically (40). Although the second RPH domain (our ΔRPH1) of the chloroplast has low RNA degradation activity of nonpolyadenylated RNA, it has high activity for polyadenylated RNA (40), which explains the efficiency of the ΔRPH1 construct in degrading human polyadenylated mRNAs. The RPH domains themselves can bind to RNA, and the PNPase domain is also involved in RNA binding, which explains the preservation of the RNA degradation activity of the ΔC-term construct, which lacks the KH and S1 RNA binding domains. Current studies are determining the effects of mutation in specific important and evolutionary conserved amino acid residues of hPNPase^{OLD-35}, especially those surrounding the tungsten binding region implicated in the enzymatic activity of the bacterial protein (19).

A unique and potentially significant finding is that hPNPase^{OLD-35} displays specific degradation activity for c-*myc* mRNA. The 3′ stem-loop structure of an RNA species determines the enzymatic activity of PNPases (40). It is of significant interest to see whether there exists a difference between the 3′ secondary structure of c-*myc* and other mRNAs, such as GAPDH and GADD34 mRNAs, that facilitates its degradation by hPNPase^{OLD-35}. PNPases function as a homotrimer (2), and our findings suggest that hPNPase^{OLD-35} also multimerizes. However, the deletion mutants that do not multimerize still retain their specific mRNA degradation activity. We can rule out the involvement of a c-*myc*-specific RNA binding protein regulating the activity of hPNPase^{OLD-35}, since our in vitro RNA degradation assays, which contained a single protein, could effectively achieve RNA degradation. Elucidation and comparison of three-dimensional models of c-*myc* and other mRNAs might provide insights into the specific RNA degradation activity of hPNPase^{OLD-35}.

Structure analysis and localization studies reveal that hPNPase^{OLD-35} is a predominantly mitochondrial protein (28, 31), thereby provoking the obvious question as to how hPNPase^{OLD-35} might degrade a cytoplasmic target mRNA, such as c-*myc*. By fractionation and immunofluorescence analyses, we demonstrate that, although the primary site of localization of hPNPase^{OLD-35} is the mitochondria, a considerable amount of the protein is also present in the cytoplasmic fraction of the cell. Similarly, ΔRPH2 and ΔC-term, which retain the mitochondrial localization signal, are also mainly localized in mitochondria, although low but detectable levels are still found in the cytoplasm. ΔRPH1 and ΔRPH1+2, lacking the mitochondrial localization signal, were located in the cytoplasm although a very low level of ΔRPH1 was also evident in the mitochondria. This is not because of cross-contamination, which was confirmed by mutually exclusive expression of cytochrome *c* and actin in mitochondria and cytoplasmic fractions, respectively. These findings suggest the existence of a potential cytoplasmic-mitochondrial shuttling of hPNPase^{OLD-35} that might be regulated by chaperone proteins. Further studies designed to identify and define interacting partners of hPNPase^{OLD-35} will help address this important question.

Adenovirus-mediated delivery usually results in robust transgene expression, which raises the important question of whether the senescence-inducing effect of Ad.*hPNPase^{old-35}* is a genuine physiological phenomenon. We have observed that there is a comparable level of hPNPase^{OLD-35} upon IFN-β treatment and with Ad.*hPNPase^{old-35}* infection, suggesting that the senescence phenotype observed with hPNPase^{OLD-35} is indeed a physiologically relevant event. Bacterial PNPase autocontrols its expression posttranscriptionally by degrading

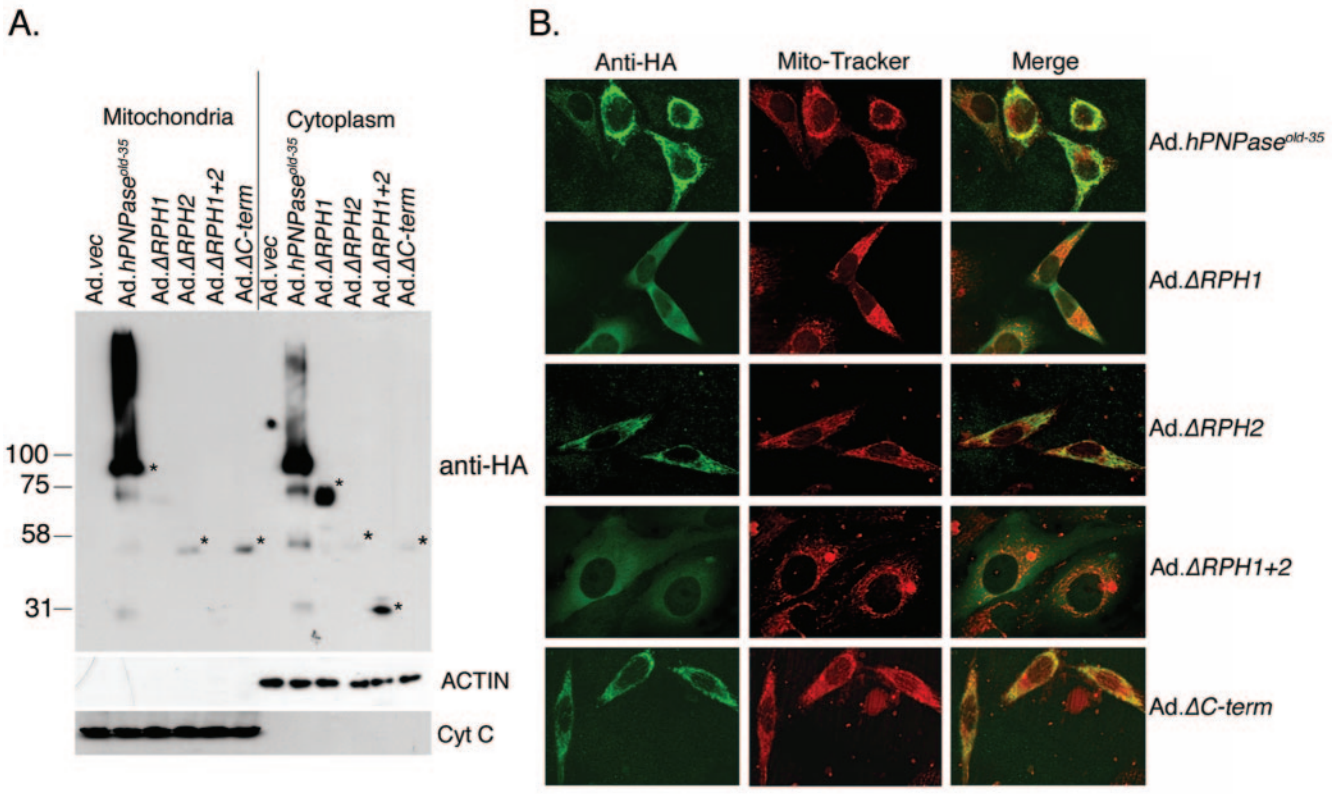

FIG. 7. Distribution of hPNPase^{OLD-35} and its deletion mutants in mitochondria and cytoplasmic compartments. A. HO-1 cells were infected with the indicated Ad, and cell fractionation was performed 36 h later. The expressions of the indicated proteins were detected by Western blot analyses. The asterisks indicate the specific bands in the corresponding lanes. B. HO-1 cells were infected with the indicated Ad and, 36 h later, loaded with MitoTracker, stained with anti-HA antibody, and visualized using a confocal laser scanning microscope.

its own mRNA (20). Although not yet confirmed for hPNPase^{OLD-35}, this posttranscriptional control might explain the restricted expression level of hPNPase^{OLD-35}, even with adenovirus-mediated delivery of this enzyme.

CDKIs, especially p16^{INK4A} and p21$^{CIP1/WAF-1/MDA-6}$, are intimately involved in the process of cellular senescence (1, 36). *hPNPase^{old-35}*-induced senescence is associated with an increase in p27^{KIP1} and a decrease in p21$^{CIP1/WAF-1/MDA-6}$, a phenomenon that is observed in two other models of senescence-like growth arrest, one resulting from iron chelation in hepatocytes and the other a consequence of inhibition of the phosphoinositide-3-kinase pathway in mouse embryo fibroblasts (6, 41). The involvement of p16^{INK4A} is ruled out as an essential component of this process because HO-1 cells do not express the p16^{INK4A} protein. The increase in p27^{KIP1} is most likely secondary to the decrease in c-*myc* that controls p27^{KIP1} expression at multiple levels, including repression of transcription and facilitation of ubiquitination and subsequent degradation (26, 27, 39). Myc plays an important role in controlling the cell cycle (14). It promotes entry into the S phase and shortens the G_1 phase. We observed that downreguation of c-*myc* by *hPNPase^{old-35}* resulted in a corresponding increase in Mad1 and this particular shift from a MYC-MAX transcriptional activator to a MAD1-MAX transcriptional repressor might be important for mediating the plethora of effects promulgated by *hPNPase^{old-35}*. However, since overexpression of Myc could not provide complete protection against *hPNPase^{old-35}*-mediated growth inhibition, additional targets of *hPNPase^{old-35}* are likely to exist that might be involved in mediating its effects. While the effect of *hPNPase^{old-35}* on c-*myc* is direct, its effect on MAD1 is probably indirect via additional targets, downregulation of which might lead to derepression of MAD1 expression.

In summary, we now confirm the importance of the RPH domains in hPNPase^{OLD-35} in inducing senescence, an event that is unique in its molecular mechanism and is critical for regulating organismal homeostasis. These studies provide unique perspectives on the molecular mechanism of senescence and the structure-function relationship of hPNPase^{OLD-35}. Crystallization of hPNPase^{OLD-35} and comparison of its crystal structure to that of the *PNPase* proteins of other species will directly facilitate identification of important residues mediating catalytic and senescence-inducing activity. Of added significance, the development of an animal model conditionally overexpressing *hPNPase^{old-35}* will provide valuable insights into the involvement of *hPNPase^{old-35}* in in vivo senescence.

ACKNOWLEDGMENTS

This study was supported in part by the Samuel Waxman Cancer Research Foundation and the Chernow Endowment. P.B.F. is the Michael and Stella Chernow Urological Cancer Research Scientist and an SWCRF Investigator.

REFERENCES

1. **Alcorta, D. A., Y. Xiong, D. Phelps, G. Hannon, D. Beach, and J. C. Barrett.** 1996. Involvement of the cyclin-dependent kinase inhibitor p16 (INK4a) in replicative senescence of normal human fibroblasts. Proc. Natl. Acad. Sci. USA **93:**13742–13747.
2. **Baginsky, S., A. Shteiman-Kotler, V. Liveanu, S. Yehudai-Resheff, M. Bellaoui, R. E. Settlage, J. Shabanowitz, D. F. Hunt, G. Schuster, and W. Gruissem.** 2001. Chloroplast PNPase exists as a homo-multimer enzyme complex that is distinct from the *Escherichia coli* degradosome. RNA **7:**1464–1475.
3. **Campisi, J.** 1992. Gene expression in quiescent and senescent fibroblasts. Ann. N. Y. Acad. Sci. **663:**195–201.
4. **Carpousis, A. J., G. Van Houwe, C. Ehretsmann, and H. M. Krisch.** 1994. Copurification of *E. coli* RNAase E and PNPase: evidence for a specific association between two enzymes important in RNA processing and degradation. Cell **76**:889–900.
5. **Chin, L.** 2003. The genetics of malignant melanoma: lessons from mouse and man. Nat. Rev. Cancer **3:**559–570.
6. **Collado, M., R. H. Medema, I. Garcia-Cao, M. L. Dubuisson, M. Barradas, J. Glassford, C. Rivas, B. M. Burgering, M. Serrano, and E. W. Lam.** 2000. Inhibition of the phosphoinositide 3-kinase pathway induces a senescence-like arrest mediated by p27Kip1. J. Biol. Chem. **275:**21960–21968.
7. **Deutscher, M. P.** 1993. Promiscuous exoribonucleases of *Escherichia coli*. J. Bacteriol. **175:**4577–4583.
8. **Deutscher, M. P.** 1993. Ribonuclease multiplicity, diversity, and complexity. J. Biol. Chem. **268:**13011–13014.
9. **Deutscher, M. P., and Z. Li.** 2001. Exoribonucleases and their multiple roles in RNA metabolism. Prog. Nucleic Acid Res. Mol. Biol. **66:**67–105.
10. **Dimri, G. P., X. Lee, G. Basile, M. Acosta, G. Scott, C. Roskelley, E. E. Medrano, M. Linskens, I. Rubelj, O. Pereira-Smith, et al.** 1995. A biomarker that identifies senescent human cells in culture and in aging skin in vivo. Proc. Natl. Acad. Sci. USA **92:**9363–9367.
11. **Fisher, P. B., and S. Grant.** 1985. Effects of interferon on differentiation of normal and tumor cells. Pharmacol. Ther. **27:**143–166.
12. **Fisher, P. B., D. R. Prignoli, H. Hermo, Jr., I. B. Weinstein, and S. Pestka.** 1985. Effects of combined treatment with interferon and mezerein on melanogenesis and growth in human melanoma cells. J. Interferon Res. **5:**11–22.
13. **Graham, G. M., L. Guarini, T. A. Moulton, S. Datta, S. Ferrone, P. Giacomini, R. S. Kerbel, and P. B. Fisher.** 1991. Potentiation of growth suppression and modulation of the antigenic phenotype in human melanoma cells by the combination of recombinant human fibroblast and immune interferons. Cancer Immunol. Immunother. **32:**382–390.
14. **Grandori, C., S. M. Cowley, L. P. James, and R. N. Eisenman.** 2000. The Myc/Max/Mad network and the transcriptional control of cell behavior. Annu. Rev. Cell Dev. Biol. **16:**653–699.
15. **Grunberg-Manago, M.** 1999. Messenger RNA stability and its role in control of gene expression in bacteria and phages. Annu. Rev. Genet. **33:**193–227.
16. **Guarini, L., G. M. Graham, H. Jiang, S. Ferrone, S. Zucker, and P. B. Fisher.** 1992. Modulation of the antigenic phenotype of human melanoma cells by differentiation-inducing and growth-suppressing agents. Pigment Cell Res. Suppl. **2:**123–131.
17. **Hayflick, L.** 1976. The cell biology of human aging. N. Engl. J. Med. **295:**1302–1308.
18. **Holmes, M., E. Rosenberg, and K. Valerie.** 2003. Adenovirus expressing p53. Methods Mol. Biol. **234:**1–16.
19. **Jarrige, A., D. Brechemier-Baey, N. Mathy, O. Duche, and C. Portier.** 2002. Mutational analysis of polynucleotide phosphorylase from *Escherichia coli*. J. Mol. Biol. **321:**397–409.
20. **Jarrige, A. C., N. Mathy, and C. Portier.** 2001. PNPase autocontrols its expression by degrading a double-stranded structure in the pnp mRNA leader. EMBO J. **20:**6845–6855.
21. **Jiang, H., Z. Z. Su, J. Boyd, and P. B. Fisher.** 1993. Gene expression changes associated with reversible growth suppression and the induction of terminal differentiation in human melanoma cells. Mol. Cell. Differ. **1:**41–66.
22. **Kelly, K. O., N. B. Reuven, Z. Li, and M. P. Deutscher.** 1992. RNase PH is essential for tRNA processing and viability in RNase-deficient *Escherichia coli* cells. J. Biol. Chem. **267:**16015–16018.
23. **Leszczyniecka, M., R. DeSalle, D. C. Kang, and P. B. Fisher.** 2004. The origin of polynucleotide phosphorylase domains. Mol. Phylogenet. Evol. **31:**123–130.
24. **Leszczyniecka, M., D. C. Kang, D. Sarkar, Z. Z. Su, M. Holmes, K. Valerie, and P. B. Fisher.** 2002. Identification and cloning of human polynucleotide phosphorylase, hPNPase^{old-35}, in the context of terminal differentiation and cellular senescence. Proc. Natl. Acad. Sci. USA **99:**16636–16641.
25. **Leszczyniecka, M., Z. Z. Su, D. C. Kang, D. Sarkar, and P. B. Fisher.** 2003. Expression regulation and genomic organization of human polynucleotide phosphorylase, hPNPase^{old-35}, a type I interferon inducible early response gene. Gene **316:**143–156.
26. **Obaya, A. J., M. K. Mateyak, and J. M. Sedivy.** 1999. Mysterious liaisons: the relationship between c-Myc and the cell cycle. Oncogene **18:**2934–2941.
27. **O'Hagan, R. C., M. Ohh, G. David, I. M. de Alboran, F. W. Alt, W. G. Kaelin, Jr., and R. A. DePinho.** 2000. Myc-enhanced expression of Cul1 promotes ubiquitin-dependent proteolysis and cell cycle progression. Genes Dev. **14:**2185–2191.
28. **Piwowarski, J., P. Grzechnik, A. Dziembowski, A. Dmochowska, M. Minczuk, and P. P. Stepien.** 2003. Human polynucleotide phosphorylase, hPNPase, is localized in mitochondria. J. Mol. Biol. **329:**853–857.
29. **Raijmakers, R., W. V. Egberts, W. J. van Venrooij, and G. J. Pruijn.** 2002. Protein-protein interactions between human exosome components support the assembly of RNase PH-type subunits into a six-membered PNPase-like ring. J. Mol. Biol. **323:**653–663.
30. **Reuven, N. B., and M. P. Deutscher.** 1993. Substitution of the 3′ terminal adenosine residue of transfer RNA in vivo. Proc. Natl. Acad. Sci. USA **90:**4350–4353.
31. **Sarkar, D., I. V. Lebedeva, L. Emdad, D. C. Kang, A. S. Baldwin, Jr., and P. B. Fisher.** 2004. Human polynucleotide phosphorylase (hPNPase^{old-35}): a potential link between aging and inflammation. Cancer Res. **64:**7473–7478.
32. **Sarkar, D., M. Leszczyniecka, D. C. Kang, I. V. Lebedeva, K. Valerie, S. Dhar, T. K. Pandita, and P. B. Fisher.** 2003. Down-regulation of Myc as a potential target for growth arrest induced by human polynucleotide phosphorylase (hPNPase^{old-35}) in human melanoma cells. J. Biol. Chem. **278:**24542–24551.
33. **Sarkar, D., Z. Z. Su, I. V. Lebedeva, M. Sauane, R. V. Gopalkrishnan, K. Valerie, P. Dent, and P. B. Fisher.** 2002. *mda*-7 (IL-24) mediates selective apoptosis in human melanoma cells by inducing the coordinated overexpression of the GADD family of genes by means of p38 MAPK. Proc. Natl. Acad. Sci. USA **99:**10054–10059.
34. **Serrano, M., and M. A. Blasco.** 2001. Putting the stress on senescence. Curr. Opin. Cell Biol. **13:**748–753.
35. **Sherwood, S. W., D. Rush, J. L. Ellsworth, and R. T. Schimke.** 1988. Defining cellular senescence in IMR-90 cells: a flow cytometric analysis. Proc. Natl. Acad. Sci. USA **85:**9086–9090.
36. **Stein, G. H., L. F. Drullinger, A. Soulard, and V. Dulic.** 1999. Differential roles for cyclin-dependent kinase inhibitors p21 and p16 in the mechanisms of senescence and differentiation in human fibroblasts. Mol. Cell. Biol. **19:**2109–2117.
37. **Symmons, M. F., G. H. Jones, and B. F. Luisi.** 2000. A duplicated fold is the structural basis for polynucleotide phosphorylase catalytic activity, processivity, and regulation. Structure Fold. Des. **8:**1215–1226.
38. **Symmons, M. F., M. G. Williams, B. F. Luisi, G. H. Jones, and A. J. Carpousis.** 2002. Running rings around RNA: a superfamily of phosphate-dependent RNases. Trends Biochem. Sci. **27:**11–18.
39. **Yang, W., J. Shen, M. Wu, M. Arsura, M. FitzGerald, Z. Suldan, D. W. Kim, C. S. Hofmann, S. Pianetti, R. Romieu-Mourez, L. P. Freedman, and G. E. Sonenshein.** 2001. Repression of transcription of the p27(Kip1) cyclin-dependent kinase inhibitor gene by c-Myc. Oncogene **20:**1688–1702.
40. **Yehudai-Resheff, S., V. Portnoy, S. Yogev, N. Adir, and G. Schuster.** 2003. Domain analysis of the chloroplast polynucleotide phosphorylase reveals discrete functions in RNA degradation, polyadenylation, and sequence homology with exosome proteins. Plant Cell **15:**2003–2019.
41. **Yoon, G., H. J. Kim, Y. S. Yoon, H. Cho, I. K. Lim, and J. H. Lee.** 2002. Iron chelation-induced senescence-like growth arrest in hepatocyte cell lines: association of transforming growth factor beta1 (TGF-beta1)-mediated p27Kip1 expression. Biochem. J. **366:**613–621.
42. **Zuo, Y., and M. P. Deutscher.** 2001. Exoribonuclease superfamilies: structural analysis and phylogenetic distribution. Nucleic Acids Res. **29:**1017–1026.